DOI: https://doi.org/10.33103/uot.ijccce.24.2.1

Computed Torque-NN-GWO Dynamic Hybrid Control of Manipulator Robotic Arm

Rafeaf J. Salman[1], Hassan M. Alwan[2], Mohammed Abais Yousif [3], Ali Mahmood Abdullah[4]
[1]*Al-Musayyib Technical Institute, Al-Furat Al-Awsat Technical University, Iraq*
[2]*Department of Mechanical Engineering, University of Technology, Baghdad, Iraq*
[3,4]*Department of Electrical Engineering Techniques, Al-Musayyib Technical Institute, Al-Furat Al-Awsat Technical University, Iraq*
[1]*rafeaf.salman@atu.edu.iq,* [2]*20071@uotechnology.edu.iq,* [3]*inm.moh2@atu.edu.iq*
[4]*ali.abdullah@atu.edu.iq*

Abstract— *Robotics involves designing, simulating, and controlling robots for various industries and daily tasks. Manipulator arm robots are precisionoriented industrial robots designed for one-plane movement. Planar robotic manipulators are used in cargo loading, assembly lines, handling radioactive materials, and military applications. In this study theoretical analysis of manipulator robot kinematics using Denavit-Hartenberg notation and the Euler-Lagrange method for a three-degree of freedom (3-DOF) system, requiring an advanced controller for accurate control. A new hybrid controller, Computed Torque Control-Neural-Network -Grey Wolf Optimization (CTC-NNGWO), is proposed for path planning of 3-DOF MR. It uses kinematics and dynamic models, computes torque magnitudes of stepper motors, and denormalizes output values from NN. MATLAB programming is used for the simulation of the theoretical result. A comparison study of CTC-NN-GWO and CTC-PSO found that CTC-NN-GWO outperforms CTC-PSO in minimizing path planning errors, the maximal value of the error of joint angular position $e_{\theta 1}$ is (0.29 rad), whereas $e_{\theta 2}$ and $e_{\theta 3}$ are approximately (0.15 rad) and (0.07 rad), respectively, also, reducing torque magnitudes, improving the performance of 3-DOF MR.*

Index Terms— *Manipulator robotic, Grey wolf, Neural network, Path planning, Computed torque***.**

I. INTRODUCTION

Robotics is the scientific study of robot design, simulation, and control [1]. It's escorted the workers in the majority of the industrial and everyday life works. Cargo loading and unloading, handling dangerous radioactive materials, automatic assembly lines, and military use are some of the applications [2]. A manipulator arm robot is a type of industrial robot that is designed to manipulate or move objects with high precision and accuracy. A manipulator robot (MR) is made up of a succession of links, each of which is attached to the link next to it via a joint. The planar MR can only move in one plane at a time. The planar MRs are prototypes that can be found in a diversity of industrial robotic regimes for aided automation as well as medicinal uses. Consequently, the investigators have been interested in manipulating an MR's position and orientation [3].

Dynamic control of a manipulator robot involves controlling the motion and forces the robot's joints to achieve desired tasks accurately and efficiently [4]. The purpose of this paper is to present the general structure of MR as well as to analyze its mathematical model in the 3-DOF-MR.

The study compared fuzzy controllers to conventional techniques like PD, PID, and computed torque control, finding the fuzzy controller offers better performance and accurate trajectory tracking. However, the robust concept was not effective and no optimization approach was used [5]. Fractional order PID offers higher degrees of freedom, efficiency, and precision compared to classical PID and

Received 14/September/2023; Accepted 23/January/2024
 ISSN (Print) 1811-9212 *ISSN (Online) 2617-3352*

DOI: https://doi.org/10.33103/uot.ijccce.24.2.1

sliding mode controllers, reducing over-shoot and stationary error [6]. Utilized the Lyapunov impedance-based technique and Particle Swarm Algorithm to optimize control robot parameters, demonstrating its efficiency in constrained motion using a 3DOF robot manipulator [1].

Computed Torque Control (CTC) is a linear control method for robotic dynamics but requires precise knowledge and isn't reliable due to unstructured and structured ambiguity, potentially causing performance devaluation [7]. Analyzes 2-DOF manipulators' behavior using Computed-Torque Control for error reduction [8]. Neural networks improve CTC for learning lumped uncertainty in robotic manipulator systems [9]. A novel approach combines CTC and Fuzzy Control for trajectory tracking into the robotic manipulator regimes having unstructured and structured ambiguity, ensuring stability and satisfactory tracking performance, provided the compensative controller is designed appropriately [10]. The application of nonlinear CTC for two-link planner robot using PD gain selection for optimal performance using MATLAB Simulink [11].

Hybrid control methodologies were used in this work. To control the joints of the manipulator arm. The CTC - PSO Coupling with CTC -NN- GWO.To integrate theoretical work and dynamic model simulation of 3-DOF MR. MATLAB Simulink application was used.

II. MATERIAL AND METHODOLOGY

A. Manipulator Robot Structure

The robot manipulator's general construction can be split into the following five main constituents: Mechanical Structure, Actuators, Sensors, Control Unit, Transmission Devices, and Data Flow. The Manipulator Robot arm (3-DOF) is made of 6061 aluminum alloy industrial weight 4kg as shown in *Fig. 1*, 3-axis with a stepper motor connected with three 298 N motor drivers, reducer, sensor, and controller. 42 planetary deceleration machines, high precision, and accuracy 0.3mm, bearing 0.5kg weight sensor. The manipulator's coordinates depend on joint angles, with the Control Unit Handling Information, Decision, and Communication simultaneously.

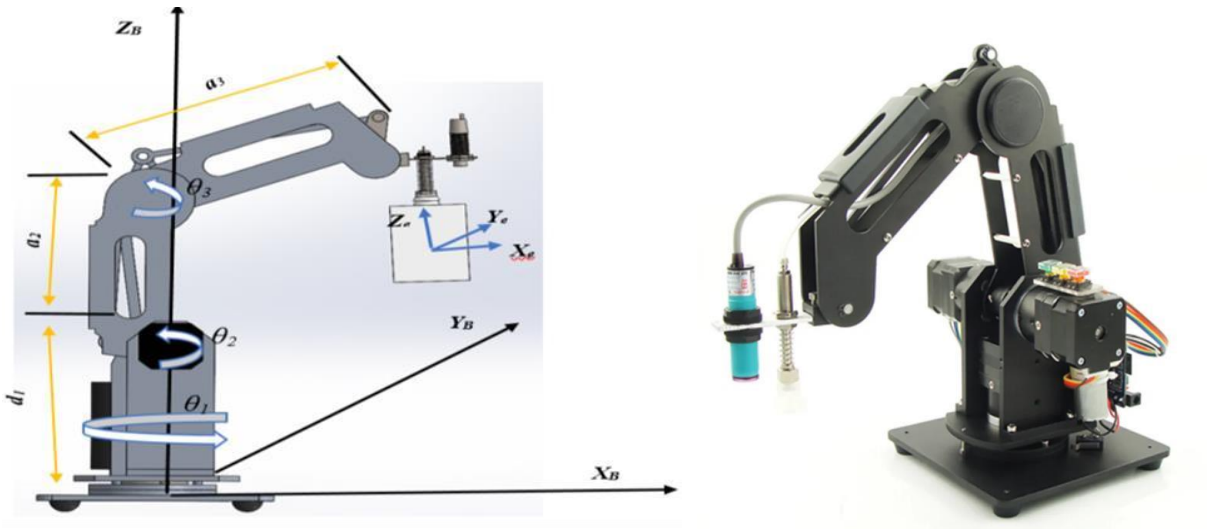

FIG. 1. THE 3-DOF MANIPULATOR ROBOT ARM.

B. The Forward kinematic Modeling of the Manipulator Robot

Kinematics is the study of the body's motion without respect for the force or moment that creates the motion. It analyzed the robot's position, orientation, velocity, and acceleration from the perspective of spatial geometry. Forward and inverse kinematics are the two types of kinematics. If the manipulator ends effector coordinates are dependent on joint angles, it's forward kinematics. Forward

Received 14/September/2023; Accepted 23/January/2024
 ISSN (Print) 1811-9212 ISSN (Online) 2617-3352

DOI: https://doi.org/10.33103/uot.ijccce.24.2.1

kinematics uses joint space measurements to determine coordinate space measures. Forward kinematics analysis maps joint space to coordinate space [12]. Denavit-Hartenberg (DH) description assigns link frames to manipulator links, producing homogenous transformation matrices, the method can be simplified by setting the z_i axis aligned with joint axis, and x_i is defined along the common normal between z_{i-1} and z_i axes pointing from z_{i-1} to z_i axis. So, the y_i axis is determined by the right-hand rule, and a DH coordinate frame is identified by four parameters a_i ,α_i , d_i, and θ_i , which are: a_i (link length), α_i (link twist), d_i (joint offset), and θ_i (joint angle)[13]. Table I shows the DH parameters for the 3-DOF manipulator robot.

TABLE I. DH PARAMETER OF ROBOT MANIPULATOR

i	**a_i(mm)**	**α_i (deg.)**	**d_i(mm)**	**θi**	**θ_i *range* (deg)**
1	0	90	d_1	θ_1	0-270
2	a_2	0	0	θ_2	0-120
3	a_3	0	0	θ_3	0-120

According to the DH convention, the transformation between two adjacent coordinate frames is denoted by:

$$ {}^{i-1}_{i}T = \begin{bmatrix} c\theta_i & -s\theta_i c\alpha_i & s\theta_i s\alpha_i & a_i c\theta_i \\ s\theta_i & c\theta_i c\alpha_i & -c\theta_i s\alpha_i & a_i s\theta_i \\ 0 & s\alpha_i & c\alpha_i & d_i \\ 0 & 0 & 0 & 1 \end{bmatrix} \quad (1) $$

$$ {}^{0}_{1}T = \begin{bmatrix} c_1 & -s_1 & 0 & 0 \\ s_1 & c_1 & 0 & 0 \\ 0 & 0 & 1 & d_1 \\ 0 & 0 & 0 & 1 \end{bmatrix} \quad (2) $$

$$ {}^{1}_{2}T = \begin{bmatrix} c_2 & -s_2 & 0 & a_2c_2 \\ s_2 & c_2 & 0 & a_2s_2 \\ 0 & 0 & 1 & 0 \\ 0 & 0 & 0 & 1 \end{bmatrix} \quad (3) $$

$$ {}^{2}_{3}T = \begin{bmatrix} c_3 & -s_3 & 0 & a_3c_3 \\ s_3 & c_3 & 0 & a_3s_3 \\ 0 & 0 & 1 & 0 \\ 0 & 0 & 0 & 1 \end{bmatrix} \quad (4) $$

$$ {}^{0}_{2}T = {}^{0}_{1}T * {}^{1}_{2}T = \begin{bmatrix} c_1c_2 & -c_1s_1 & s_1 & a_2c_2c_1 \\ c_1s_2 & c_1c_2 & c_1 & a_2c_2s_1 \\ 0 & 0 & 1 & d_1 + a_2s_2 \\ 0 & 0 & 0 & 1 \end{bmatrix} \quad (5) $$

Where:

$c_i = \cos(\theta_i)$ for $i = 1, \ldots, 3$, $s_i = \sin(\theta_i)$ for $i = 1, \ldots, 3$, $s_{23} = \sin(\theta_2 + \theta_3)$, and $c_{23} = \cos(\theta_2 + \theta_3)$.

The end-effector's net transformation to the base coordinate frame regime can be determined as follows:

Received 14/September/2023; Accepted 23/January/2024

 ISSN (Print) 1811-9212 *ISSN (Online) 2617-3352*

DOI: https://doi.org/10.33103/uot.ijccce.24.2.1

$$ {}^{0}_{3}\mathrm{T} = {}^{0}_{1}\mathrm{T}\ {}^{1}_{2}\mathrm{T}\ {}^{2}_{3}\mathrm{T} \tag{6} $$

$$ {}^{0}_{3}\mathrm{T} \begin{bmatrix} c_1c_{23} & -c_1s_{23} & s_1 & c_1(a_2c_2 + a_3c_{23}) \\ s_1c_{23} & -s_1s_{23} & c_1 & s_1(a_2c_2 + a_3c_{23}) \\ s_{23} & c_{23} & 0 & (d_1 + a_2s_2 + a_3s_{23}) \\ 0 & 0 & 0 & 1 \end{bmatrix} $$

The forward kinematics are calculated by using DH Parameters of the Robot Manipulator [13],[14] and the transformation matrix in Eq.6 as shown in Eq.7:

$$ \begin{aligned} X_e &= (a_2 * c_2 + a_3 * c_{23}) * c_1 \\ Y_e &= (a_2 * c_2 + a_3 * c_{23}) * s_1 \\ Z_e &= d_1 + (a_2 * s_2 + a_3 * s_{23}) \end{aligned} \tag{7} $$

C. The Dynamic Modeling of 3-DOF MR

The study of robotic systems' dynamic behavior necessitates the use of a mathematical model that allows designers to predict torque change at joints. The manipulator's robot dynamic model was developed in this section. A 3-DOF (Degree of Freedom) manipulator robot consists of three joints that are capable of rotating or moving in one of three directions. The energy-based Lagrange-Euler technique, as shown in the following equation, is a standard strategy for constructing the mathematical model for a dynamic system: [15].

$$ (q)\ddot{q}_i - C(q, \dot{q})\dot{q}_i + G(q) = \tau_i \tag{8} $$

(q) is the $n \times n$ the 3-DOF MR system inertia torques matrix.
C(q, $\dot{q}$) is an $n \times n$ the 3-DOF MR system centrifugal as well as Coriolis torques matrix.
G(q) represents the gravitational torque's $n \times 1$ vector.

It is difficult to develop a 3-DOF MR mathematical model, especially for a greatly redundant manipulator robot, a set of highly nonlinear and coupled differential equations was the final model. The 3-DOF MR depicted in *Fig. 1* is used as a model of a manipulator-articulated serial robot. This system of the robot contains (3) links, each one having its mass (m) and length (a_i), which revolve the angles (θ_2) and (θ_3) into a three-dimensional operating space. Angle $\theta 1$ is an angle at which the whole manipulator links rotate about the axis Z_L. To explain the dynamics of a three-degree of freedom (3-DOF) robotic regime, a group of (3) differential equations is required. And, the derivation of such three equations needs the assessment of potential as well as kinetic energy purposes for the whole of the linkages of the robot. Take a look at *Fig. 2*, which depicts the manipulator robot arm in an XYZ local coordinate instantaneous, θ_1 is a rotated angle at a given time step about the Z_B local axis.

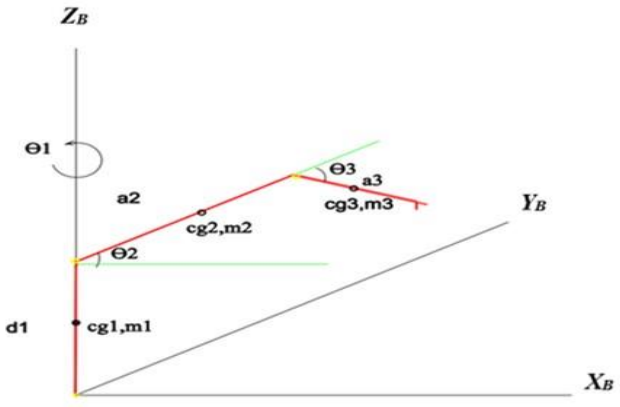

FIG. 2. SIDE VIEW OF THE 3-DOF MR.

Received 14/September/2023; Accepted 23/January/2024
 ISSN (Print) 1811-9212 ISSN (Online) 2617-3352

DOI: https://doi.org/10.33103/uot.ijccce.24.2.1

Beginning at the manipulator arm base, the base mass center located at (x_1, y_1, z_1) into the (X_B Y_B Z_B) coordinate has a linear and a rotating movement about the base, therefore, one can be calculated the kinetic energy (T_1), and the potential energy (U_1) as follows:

$$T_{mi} = 1/2 * m_i * V_i^2 + 1/2 * I_i * W_i^2 \quad (9)$$

$$V_i^2 = \dot{x}_i^2 + \dot{y}_i^2 + \dot{z}_i^2 \quad (10)$$

For the base:

$$X_1 = 0 \Rightarrow \dot{X}_1 = 0,$$

$$Y_1 = 0 \Rightarrow \dot{Y}_1 = 0, Z_1 = r_{c1} \Rightarrow \dot{Z}_1 = 0$$

$$V_{12} = \dot{X}_{12} + \dot{Y}_{12} + \dot{Z}_{12}$$

$$U_1 = 0$$

$$T_1 = 1/2 * m_1 V_1^2 + 1/2 * I_{1z} \dot{\theta}_1^2$$

For link 2:

$$X_2 = r_{c2} c_2 c_1$$

$$\dot{X}_2 = -r_{c2} * [s_2\, c_1 \dot{\theta}_2 + c_2\, s_1 \dot{\theta}_1]$$

$$Y_2 = r_{c2}\, c_2\, s_1$$

$$\dot{Y}_2 = r_{c2}[c_2\, c_1 \dot{\theta}_1 - s_2\, s_1 \dot{\theta}_2]$$

$$Z_2 = d_1 + r_{c2} s_2$$

$$\dot{Z}_2 = r_{c2} c_2\, \dot{\theta}_2$$

$$V_{22} = \dot{X}_{22} + \dot{Y}_{22} + \dot{Z}_{22}$$

$$U_2 = m_2(d_1 + r_{c2}\, s_2)$$

$$T_2 = 1/2 * m_2 V_2^2 + 1/2 * I_{2z} \dot{\theta}_1^2 + 1/2 * I_{2y} \dot{\theta}_2^2$$

For link 3:

$$X_3 = (a_2 c_2 + r_{c3}\, c_{23})_1$$

$$\dot{X}_3 = -(a_2 c_2 + r_{c3} c_{23}) s_1 \dot{\theta}_1 - c_1(a_2 s_2 \dot{\theta}_2 + r_{c3} s_{23}(\dot{\theta}_2 + \dot{\theta}_3)$$

$$Y_3 = (a_2 c_2 + r_{c3}\, c_{23})_1$$

$$\dot{Y}_3 = (a_2 c_2 + r_{c3}\, c_{23})_1 \dot{\theta}_1 - s_1\,(a_2 s_2 \dot{\theta}_2 + r_{c3}\, s_{23}(\dot{\theta}_2 + \dot{\theta}_3))$$

$$Z_3 = d_1 + a_2 s_2 + r_{c3} s_{23}$$

$$\dot{Z}_3 = a_2 c_2 \dot{\theta}_2 + r_{c3} c_{23}(\dot{\theta}_2 + \dot{\theta}_3)$$

$$V_{32} = \dot{X}_{32} + \dot{Y}_{32} + \dot{Z}_{32}$$

$$U_3 = -m_3(d_1 + a_2 s_2 + r_{c3} s_{23})$$

$$T_3 = 1/2 * m_3 V_3^2 + 1/2 * I_{3z} \dot{\theta}_1^2 + 1/2 * I_{3y}\,(\dot{\theta}_2 + \dot{\theta}_3)^2$$

For mass M on the end effector:

Received 14/September/2023; Accepted 23/January/2024
 ISSN (Print) 1811-9212 ISSN (Online) 2617-3352

DOI: https://doi.org/10.33103/uot.ijccce.24.2.1

$$X_M = x_c + (a_2c_2 + a_3c_{23})_1$$

$$X^{\cdot}_M = -(a_2c_2 + a_3c_{23})s_1\theta^{\cdot}_1 - c_1\,(a_2s_2\theta^{\cdot}_2 + a_3s_{23}(\theta^{\cdot}_2 + \theta^{\cdot}_3))$$

$$Y_M = (a_2c_2 + a_3c_{23})_1$$

$$Y^{\cdot}_M = (a_2c_2 + a_3c_{23})_1\theta^{\cdot}_1 - s_1\,(a_2s_2\theta^{\cdot}_2 + a_3s_{23}(\theta^{\cdot}_2 + \theta^{\cdot}_3))$$

$$Z_M = d_1 + a_2s_2 + a_3s_{23}$$

$$Z^{\cdot}_M = a_2c_2\theta^{\cdot}_2 + a_3c_{23}(\theta^{\cdot}_2 + \theta^{\cdot}_3)$$

$$V_{M2} = X^{\cdot}_{M2} + Y^{\cdot}_M + Z^{\cdot}_M$$

$$U_{\mathrm{M}} = -\mathrm{M}(d_1 + a_2s_2 + a_2s_{23})$$

$$T_M = 1/2 * \mathrm{M} * V_M^2 + 1/2 * I_{\mathrm{M}z}\theta^{\cdot}_1{}^2 + 1/2 * I_{My}\,(\theta^{\cdot}_2 + \theta^{\cdot}_3)^2$$

Eq. (11) provides the Lagrange equation of motion for the component system:

$$L=T_1 + T_2 + T_3 + T_M - (U_1 + U_2 + U_3 + U_M) \tag{11}$$

$$\frac{\partial}{\partial t}\left(\frac{\partial L}{\partial \dot{\theta}_1}\right) - \frac{\partial L}{\partial \theta_1} = \tau_1$$

$$\frac{\partial}{\partial t}\left(\frac{\partial L}{\partial \dot{\theta}_2}\right) - \frac{\partial L}{\partial \theta_2} = \tau_2$$

$$\frac{\partial}{\partial t}\left(\frac{\partial L}{\partial \dot{\theta}_3}\right) - \frac{\partial L}{\partial \theta_3} = \tau_3$$

$$\mathrm{M} = \begin{bmatrix} m_{11} & m_{12} & m_{13} \\ m_{21} & m_{22} & m_{23} \\ m_{31} & m_{32} & m_{33} \end{bmatrix},\ C = \begin{bmatrix} c_{11} & c_{12} & c_{13} \\ c_{21} & c_{22} & c_{23} \\ c_{31} & c_{32} & c_{33} \end{bmatrix}$$

$$m_{11} = I_{z1} + I_{z2} + I_{z_3} + I_{Mz} + Mc_1^2(a_3c_{23} + a_2c_2)^2 + m_3c_1^2\left(a_2c_2 + r_{c_3}c_{23}\right) + m_2r_{c2}^2c_1^2c_2^2$$

$$m_{12} = m_{21} = -m_2c_1c_2s_1s_2r_{c2}^2 - m_3c_1s_1(r_{c3}c_{23} + a_2c_2) * (a_2c_2 + r_{c3}s_{23}) - Mc_1s_1(a_2c_2 + a_3c_{23}) * (a_2s_2 + a_3s_{23})$$

$$m_{13} = m_{13} = -Ma_3c_1s_1s_{23}(a_2c_2 + a_3c_{23}) - m_3r_{c3}c_1s_1s_{23}\,(a_2c_2 + r_{c3}c_{23})$$

$$m_{22} = I_{y_2} + I_{y_3} + I_{yM} + (\,m_3(* (2s_1^2(a_2s_2 + r_3s_{23})^2 + 2(a_2c_2 + r_{c3} * c_{23})^2 + 2 * (r_{c3} * \sin(2\theta_2{+}\theta_3) + a_2 * \sin(2\theta_2)^2/2 + (M * (2s_1^2 * (a_2s_2 + a_3s_{23})^2 + 2(a_2c_2 + a_3c_{23})^2 + 2 * (a_3\sin(2\theta_2{+}\theta_3) + a_2\sin(2\theta_2)^2/2 + \left(m_2 * \left(2r_{c_2}^2c_2^2 + 2r_{c_2}^2 * \sin(2\theta_2)^2 + 2r_{c_2}^2 * s_1^2s_2^2\right)\right)/_2$$

$$m_{23} = m_{32} = I_{y_3} + I_{yM} + \Big(M \cdot \Big(2 * (a_3\sin(2\theta_2{+}\theta_3) + a_2\sin(2\theta_2) * \Big(\big(a_3\sin(2\theta_2{+}\theta_3)\big)/ 2\ -\big(a_3 * \sin(\theta_3)\big)/2 + 2a_3c_{23} \times (a_3c_{23} + a_2c_2) + 2 * a_3s_1^2s_{23}(a_2s_2 + a_3s_{23})\Big)\Big)/2 + m_3\Big(2 * \big(r_{c_2} * \sin(2\theta_2{+}\theta_3) + a_2 * \sin(2\theta_2\big) * (r_{c3}\sin(2\theta_2 + \theta_3))/2 - \big(r_{c_3} * \sin(\tfrac{\theta_3}{2} + 2r_{c_3} * c_{23} * (a_2c_2 + r_{c3}c_{23}) + 2r_{c3} * s_1^2s_{23} * \big(a_2s_2 + r_{c_3}s_{23}\big)\Big)\Big)/2$$

$$m_{33} = I_{y_3} + I_{yM} + \Big(m_3 * \big(2 * \big(r_{c3} * \sin(2\theta_2{+}\theta_3)\big)/2 - (r_{c3}\,s_3)/2\big)^2 + 2r_{c2}^2c_{23}^2 + 2r_{c3}^2s_1^2s_{23}^2\Big)\Big)/2 + \left(M * \left(2a_3^2 \cdot c_{23}^2 + 2 * \Big(\big(a_3\sin(2\theta_2 + \theta_3)\big)/2 - a_3\,s_3\Big)\right)^2\right)^2 + 2a_3^2s_1^2s_{23}^2/2$$

Received 14/September/2023; Accepted 23/January/2024
 ISSN (Print) 1811-9212 *ISSN (Online) 2617-3352*

DOI: https://doi.org/10.33103/uot.ijccce.24.2.1

$c_{11} = -2m_3c_1\,s_1(a_2c_2 + r_{c3}c_{23})^2 - 2Mc_1\,s_1(a_2c_2 + a_3c_{23})^2 - 2m_2r_{c2}^2c_1c_2^2s_1{*}(a_2s_2 + r_{c3}s_{23})^2 + Mc_1s_1(a_2s_2 + a_3s_{23})^2 + m_2r_{c2}c_1s_1(s_2^2\text{-}c_2^2)$

$c_{12} = c_{a21} = Ms_1^2(a_2c_2 + a_3c_{23}) * (a_2s_2 + a_3s_{33}) - Mc_1^2(a_2c_2 + a_3c_{23}) * (a_2s_2 + a_3s_{23}) - m_3c_1^2 * (a_2c_2 + r_{c3}c_{23}) * \left(a_2s_2 + r_{c_3}s_{23}\right) + m_3s_1^2(a_2c_2 + r_{c3}c_{23})(a_2s_2 + r_{c3}s_{23}) - m_2r_{c2}^2c_1^2c_2s_2 + m_2r_{c2}^2c_2s_1^2s_2$

$c_{13} = c_{a31} = m_3r_{c3}^2c_1s_1s_{23}^2 + Ma_3^2c_1s_1s_{23}^2 - Ma_3c_1c_{23}s_1(a_2c_2 + a_3c_{23}) - m_3r_{c3}c_1c_{23}s_1(a_2c_2 + r_{c3}c_{23})$

$c_{22} = (m_3 \times (4(2r_{c3}\cos(2\theta_2 + \theta_3) + 2a_2\cos(2\theta_2) * (r_{c3}\sin(2\theta_2 + \theta_3) + a_2\sin(2\theta_2) - 4 * (r_{c3}c_{23} + a_2c_2) + (a_2s_2 + r_{c3}s_{23}) + 4s_1^2(a_2c_2 + r_{c3}c_{23}) \star (a_2s_2 + r_{c3}s_{23}))\big)/2 + (m_2 \times (8r_{c2}^2\cos(2\theta_2) * \sin(2\theta_2) - 4r_{c2}^2c_2s_2 + 4r_{c2}^2c_2s_1^2s_2)\big)/2 + (M(4(2a_3\cos(2\theta_2 + \theta_3) + 2a_2\cos(2\theta_2) * (a_3\sin(2\theta_2 + \theta_3) + a_2\sin(2\theta_2) - 4(a_2c_2 + a_3c_{23}) \times (a_2s_2 + a_3s_{23}) + 4s_1^2 * (a_2c_2 + a_3c_{23})(a_2s_2 + a_3s_{23}))\big)/2$

$c_{23} = c_{32} = \big(m_3\big(2 \times \big((r_{c3}\cos(2\theta_2 + \theta_3)/2 + (r_{c3}\,c_3)/2 + (r_{c3}\sin(2\theta_2 + \theta_3) + a_2sin(2\theta_2) - 2r_{c3}s_{23}(a_2c_2 + r_{c3}c_{23}) - 2r_{c3}^2c_{23}s_{23} + 2r_{c3}cos(2\theta_2 + \theta_3) * \big(r_{c3}sin(2\theta_2 + \theta_3)\big)/2 - (r_{c3}\,s_3)/2\big) + 2r_{c3}c_{23}s_1^2(a_2s_2 + r_{c3}s_{23}) + 2r_{cs}^2c_{23}s_1^2s_{23})\big)/2 + \Big(M\Big(2 * \Big(\big(a_3cos(2\theta_2 + \theta_3)\big)/2 + (a_3\,c_3)/2\Big) * (a_3\sin(2\theta_2 + \theta_3) + a_2\sin(2\theta_2) - 2a_3^2c_3s_{23} + 2a_3\cos(2\theta_2 + \theta_3) * \Big(\big(a_3\sin(2\theta_2 + \theta_3)\big)/2 - (a_3\,s_3)/2\Big) - 2a_3s_{23}(a_2c_2 + a_3c_{23}) + 2a_2c_{23} * s_1^2 + (a_2s_2 + a_3s_{33}) + 2a_3^2c_{23}s_1^2s_{23})\Big)/2$

$c_{33} = \Big(M * (4\Big(\big(a_3\cos(2\theta_2 + \theta_3)\big)/2 + (a_3\,c_3)/2\Big) * \big(a_3\sin(2\theta_2 + \theta_3)\big)/2 - (a_3s_3)/2) - 4a_3^2c_{23}s_{23} + 4a_3^2c_{23}s_1^2s_{23})\Big)/2 + \big(m_3\big(4\big((r_{c3}\cos(2\theta_2 + \theta_3)\big)/2\big) + (r_{c3}\,c_3)/2\big) * \Big(\big(r_{c3}\sin(2\theta_2 + \theta_3)\big)/2 - (r_{c3}s_3)/2\Big) - 4r_{c3}^2c_{23}s_{23} + 4r_{c3}^2c_{23}s_1^2s_{23})\Big)/2$

$G_1 = 0$

$G_2 = -Mg(a_2c_2 + a_3c_{23}) - m_3g(a_2c_2 + r_{c3}c_{23}) - m_2g\,r_{c2}c_2$

$G_3 = -Mga_3c_{23} - m_3gr_{c3}c_{23}$

D. Path Planning Controllers Design of 3-DOF MR

Hybrid control methodologies are used in this work, with manipulator robot models explained that are CTC - PSO Coupling with CTC -NN- GWO.

Three PID controllers were required to manage the rotating speed of the processor's joints because the CTC was utilized. In the first methodology, the PID optimal values of gains (K_p, K_i, K_d) were intended by PSO. While, in the 2nd approach, where the NN determines the NN weights' first values, and the GWO calculates the gain parameters values. The following sections detail all of the control algorithms that were used:

1. Computed Torque Control (CTC)

It's a subset of nonlinear feedback linearization that has gained interest in modern systems theory [16]. When there are no external forces impacting the link between the three joints or end-effectors, eq. (8) gives the 2nd-order vector differential equation for manipulator movement in terms of the applied joint torques. CTC is utilized to replicate reality in this study by collaborating with a real robot to demonstrate the impacts of external force on the variables' location, velocity, acceleration, and torque.

Received 14/September/2023; Accepted 23/January/2024
 ISSN (Print) 1811-9212 ISSN (Online) 2617-3352

DOI: https://doi.org/10.33103/uot.ijccce.24.2.1

In the next stages, the equation of the CTC law is derived. If the desired path $\theta(t)$ for the arm manipulation is [8]:

$$(t) = \theta_d(t) - \theta(t) \quad (15)$$

Taking the error's first and second derivatives yields:

$$e^{\cdot} = \theta^{\cdot}{}_d - \theta^{\cdot}, \quad e^{\cdot\cdot} = \theta^{\cdot\cdot}{}_d - \theta^{\cdot\cdot} \quad (16)$$

Get ¨ from eq .(8) as follow :

$$\theta^{\cdot\cdot} = (\theta)^{-1}(\tau - C(\theta, \theta^{\cdot})\theta^{\cdot}) \quad (17)$$

Via transferring the $\theta^{\cdot\cdot}$ from Eq. (17) into Eq. (16), so

$$e^{\cdot\cdot} = \theta^{\cdot\cdot}{}_d + (\theta)^{-1}(C(\theta, \theta^{\cdot})\,\theta^{\cdot} - \tau) \quad (18)$$

And, the control input function is defined by:

$$u = e^{\cdot\cdot} = \theta^{\cdot\cdot}{}_d + (\theta)^{-1}(C(\theta, \theta^{\cdot})\,\theta^{\cdot} - \tau) \quad (19)$$

Also, the computed joint torque is provided via Eq. (19).

$$\tau = (\theta)(\theta^{\cdot\cdot}{}_d - u) + C(\theta, \theta^{\cdot})\,\theta^{\cdot} \quad (20)$$

Choose u as a feedback signal of PD.

$$u = -K_d e^{\cdot} - K_p e \quad (21)$$

The computed torque of the joint, which is the manipulator robot arm input, when eq. (20) is substituted for eq. (21), becomes

$$\tau = (\theta)(\theta^{\cdot\cdot}{}_d + K_d\, e^{\cdot} + K_p e) + C(\theta, \theta^{\cdot})\,\theta^{\cdot} \quad (22)$$

This is known as the CTC law.PD increases are typically used for critical damping =1[113,114] In this case:

$$K_d = 2\sqrt{K_p} \text{ and } K_p = {}^{K_4}\underline{d}^2 \quad (23)$$

The CTC is based upon the robot dynamics inversion, as well as it produces the actual acceleration vector of the joint after it is calculated from equation (22) and inserting its value into equation (17). The system's overall equations can be derived from Eq. (8) as well as Eq. (22) as follows:

$$\tau = \mathrm{M}(\theta)\,\theta^{\cdot\cdot} + C(\theta, \theta^{\cdot})\,\theta^{\cdot} = M(\theta)(\theta^{\cdot\cdot}{}_d + K_d\, e^{\cdot} + K_p e) + C(\theta, \theta^{\cdot})\,\theta^{\cdot} \quad (24)$$

$$\theta^{\cdot\cdot} = \theta^{\cdot\cdot}{}_d + K_d\, e^{\cdot} + K_p e$$

Therefore,

$$e^{\cdot\cdot} + K_d\, e^{\cdot} + K_p e = 0 \quad (25)$$

2. Particle Swarm Optimization (PSO)

The PSO method begins by creating particles at random inside the search space. With each iteration, particles with their given velocities fly throughout the search space with the hope of identifying the optimal solution. Each particle's velocity is updated depending on the current velocity of the particle, the individualized supreme solution of the particle, and the general supreme solution determined so far. Then, the positions of particles are updated iteratively depending upon the fresh velocities till the halting criteria are met [17], [18].

$$v_{it+1} = w * v_{it} + c1 * r1 \times (p_{i,} - x_{it,d}) + c2 * r2 \times (p_{g,d} - x_{it,d}) \quad (26)$$

$$x_i{}^{t,}{}^{+}{}_d{}^1 = x_i{}^{t}{}_{,d} + v_i{}^{t+1} \quad (27)$$

In Eqs. (26) and (27), the future positions and current of the i^{th} particle are $x_i{}^{t,}{}^{+}{}_d{}^1$ and $x_i{}^{t}{}_{,d}$. The particle's current velocity is the parameter $v_i{}^{t}$, and w is a weighting function that controls how the

Received 14/September/2023; Accepted 23/January/2024
 ISSN (Print) 1811-9212 ISSN (Online) 2617-3352

DOI: https://doi.org/10.33103/uot.ijccce.24.2.1

current velocity of the particle affects its upcoming velocity. And, the variable $p_{i,}$ signifies the supreme particle i solution at iteration t, while $p_{g,d}$ represents the supreme general solution so far. Also, the comparative value of the present supreme local as well as general solutions is obtained via the (2) weighting criteria (c_1 and c_2). The r_1 and r_2 values are two random numbers between [0,1] that are used to induce stochastic particle exploration throughout the search space.

3. Neural Networks (NNs)

NNs are artificial intelligence regimes that mimic biological neurons. And, NNs communicate by using a structure alike to that of biological neurons. There are two kinds of neural networks: Feed-forward networks and Feed-back networks. The feed-forward networks allow the data to flow in only one way, while the feed-back networks allow the data to return to the preceding neurons. The neural network employs (3) layers for neuron output: Input, hidden, and output, using bipolar sigmoidal activation functions. The first hidden layer has a bipolar sigmoidal activation function with a range of [0-1], while the second has a binary sigmoidal activation function. Both activation functions' essential mathematical equations are [19]:

(a) Binary Sigmoidal

$$f(net) = \frac{1}{1+e^{-net}} \tag{28}$$

(b) This activation function is connected to the tangent function and has the following fundamental formula:

$$f(net) = \frac{2}{1+e^{-net}} - 1 \tag{29}$$

4. Grey Wolf Optimizer (GWO)

GWO is a nature-inspired optimization method founded upon the conduct of grey wolf hunting. Setting an objective function, and variables, creating a pack of wolves, assessing the fitness of wolves, choosing alpha, beta, and delta wolves, as well as updating locations are all utilized to drive manipulator robots [20]. Then, the program extracts the supreme governing factors and assesses the performance in real-life or simulated circumstances. And, the study concludes with mathematical models of wolves' social structure, such as preparation, en-circling, and assaulting victim [21].

A-Social hierarchy

The algorithm of GWO is intended for improving the hunting via guiding, as well as with (ω) wolves, and trailing (3) wolves (α, β, and δ).

B-Encircling prey

During the hunt, grey wolves enclose the victim utilizing equations to model encircling behavior [21].

$$D^{\rightarrow} = \left|\vec{C} \cdot \vec{X}_p(t) - \vec{X}(t)\right|$$
$$X(t+1) = \vec{X}_p(t) - \vec{A} \cdot D^{\rightarrow} \tag{30}$$

Where, t represents the current iteration, and C are coefficient vectors, X_p is the prey position vector, and X represents the position vector of a grey wolf. The vectors and C are computed in the following manner[21]:

$$A = 2a \cdot r_1 - a$$
$$C = 2 \cdot r_2 \tag{31}$$

Received 14/September/2023; Accepted 23/January/2024
 ISSN (Print) 1811-9212 ISSN (Online) 2617-3352

DOI: https://doi.org/10.33103/uot.ijccce.24.2.1

Where, the constituents of are decreased linearly from two to zero over the course of the iteration, and r_1,r_2 represent the arbitrary vectors into [0,1].

C-Hunting

GWs can determine the positions of prey and enclose them using the signals of alpha, beta, and delta. We don't know where the best prey is in an abstract search space. To simulate hunting behavior, one saves the top three greatest options and encourages other investigators to update their positions based on the positions of the top three search agents [21].

$$D^{\rightarrow}{}_{\alpha} = |C_1 \cdot X_{\alpha} - X|, D^{\rightarrow}{}_{\beta} = |C_2 \cdot X_{\beta} - X|, D^{\rightarrow}{}_{\delta} = |C_3 \cdot X_{\delta} - X|$$

$$X_1 = X_{\alpha} - A_1 \cdot (D^{\rightarrow}{}_{\alpha}), {}_2 = X_{\beta} - A_2 \cdot (D^{\rightarrow}{}_{\beta}), X_3 = X_{\delta} - A_3 \cdot (D^{\rightarrow}{}_{\delta})$$

$$X(t+1) = \frac{\vec{X}_1 + \vec{X}_2 + \vec{X}_3}{3} \quad (32)$$

D-Attacking the pery

As previously stated, grey wolves complete the hunt by attacking the target when it stops moving. One reduces the value of to mathematically model approaching the prey. It is noted that the variation range is also reduced via a . And, in n different words, represents an arbitrary value into the interval $[-2a, 2a]$, where a is reduced from two to zero through the course of the iteration. If the arbitrary values of are into $[-1,1]$, the following location of a hunting agent can be in any location[21].

E- The search for prey (Exploration)

GWs use alpha, beta, and delta locations for finding the prey and then converging to the attack. The models of the algorithm of GWO diverge by using arbitrary values, with an emphasis on the exploration as well as the general hunt**.** And, the (~C) vector is the obstacles, encouraging the exploration as well as the local optimal avoiding. This algorithm estimates prey positions using random values and C vectors, with the factor reducing from two to zero. The candidates diverge if |A |>1 and converge if |A |<1. And, the algorithm ends via filling in a termination criterion [21].

In this study, the CTC-PSO control methodology, the PSO was espoused for computing the CTC gains factors (kp_1, kp_2, kp_3, kd_1, kd_2, and kd_3), while, in the CTC-NNGWO control methodology, the CTC gains factors were (kp_1, kp_2, kp_3, kd_1, kd_2, and kd_3) Because the outputs of NN being in the usual range (that means the values are in the [0-1] range), GWO is utilized for determining the proper scaling parameters employed for normalizing the outputs of NN. Moreover, Simulation is considered to be an important research tool in the different areas of applications, such as visualization, planning, control systems, and robotics. In this work, MATLAB/ Simulink 2021 has been used to present the theoretical robot models as well as the control theory of trajectory tracking that has been derived in this section. *Fig. 3* reveals the diagram of the general primary simulation into the MATLAB/Simulink for the initial governing mechanism.

Received 14/September/2023; Accepted 23/January/2024
 ISSN (Print) 1811-9212 *ISSN (Online) 2617-3352*

DOI: https://doi.org/10.33103/uot.ijccce.24.2.1

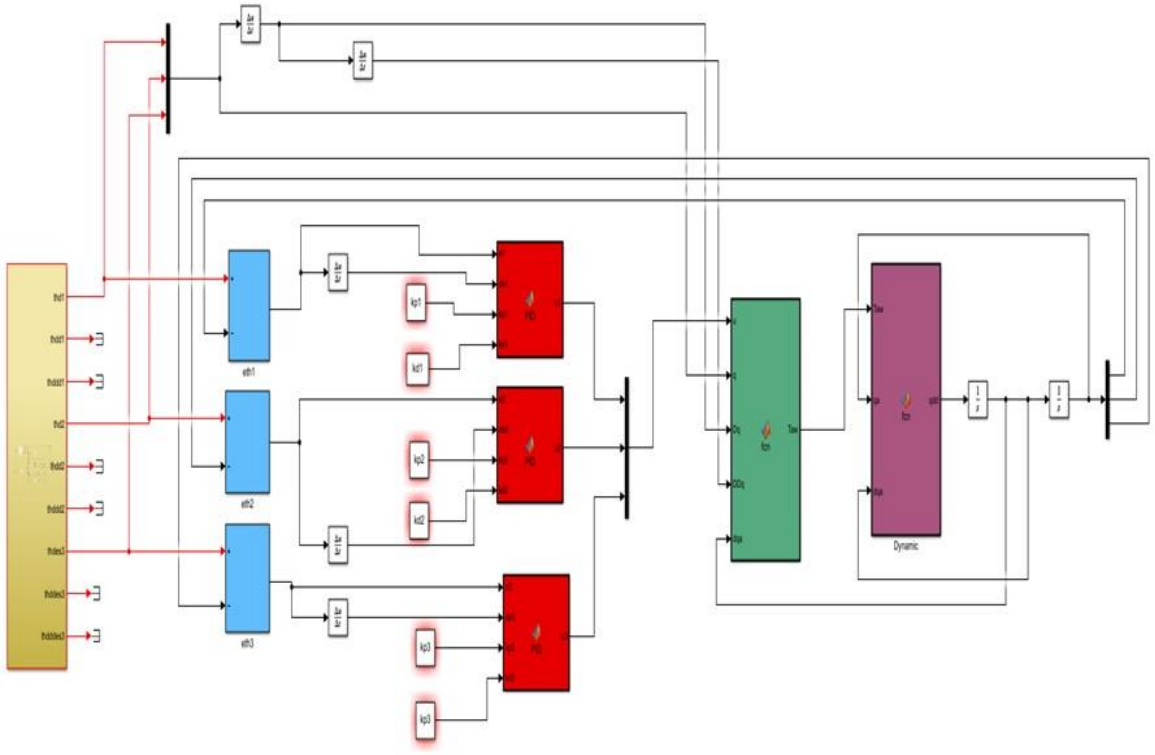

FIG. 3. DIGRAM OF THE MATLAB/SIMULINK OF CTC-PSO GOVERNING TECHNIQUE.

The desired path is shown by the yellow-colored block. The blocks with a light blue color suggest joint angle issues. The outputs of the light blue color (joint angle errors) are thought to be the inputs to the system of PID consisting of the red blocks. And, the gains (K_{p1}, K_{p2}, $K_{p3,}$ K_{d1}, K_{d2}, and K_{d3}), as well as the derivative errors of joint angle, are fed into the PID system. Furthermore, the red systems' outputs are regarded as inputs to the manipulator's computed torque, which is depicted in green. Finally, the green system outputs are the governed torques, which being thought to be the inputs to the manipulator's burgundy dynamic model.

The green boxes manifest the desired trajectory, while the red blocks represent the faults in the joint angles. The red outputs (joint angle errors) are regarded as the inputs to the NN system contained within blue blocks. The first blue block represents the N.N system's inputs, which are the joint angle errors, whereas the 2nd and 3rd blue blocks are the (2) hidden layers used in the present investigation.

The blocks (b) and (W) displayed in the preceding diagrams are the baios and the weight, respectively whose values being estimated using the technique of GWO. And, the first hidden layer's activation function is a logsig, while the second hidden layer's activation function is a tansig. The N.N produces six outputs, which indicate the gain settings of the calculated torque controller.

The (3) regimes in orange are represent the calculated torque control gains. And, the orange regimes are the errors of the velocities of joint velocities and also the controller gains factors estimated by NN. The outputs of the orange systems are regarded as inputs to the computed torque of the manipulator, which is represented in magenta. The controlled torques are the outputs of the system in magenta color, which are considered the inputs to the manipulator's dynamic model into gray color into *Fig. 4*.

Received 14/September/2023; Accepted 23/January/2024
 ISSN (Print) 1811-9212 ISSN (Online) 2617-3352

DOI: https://doi.org/10.33103/uot.ijccce.24.2.1

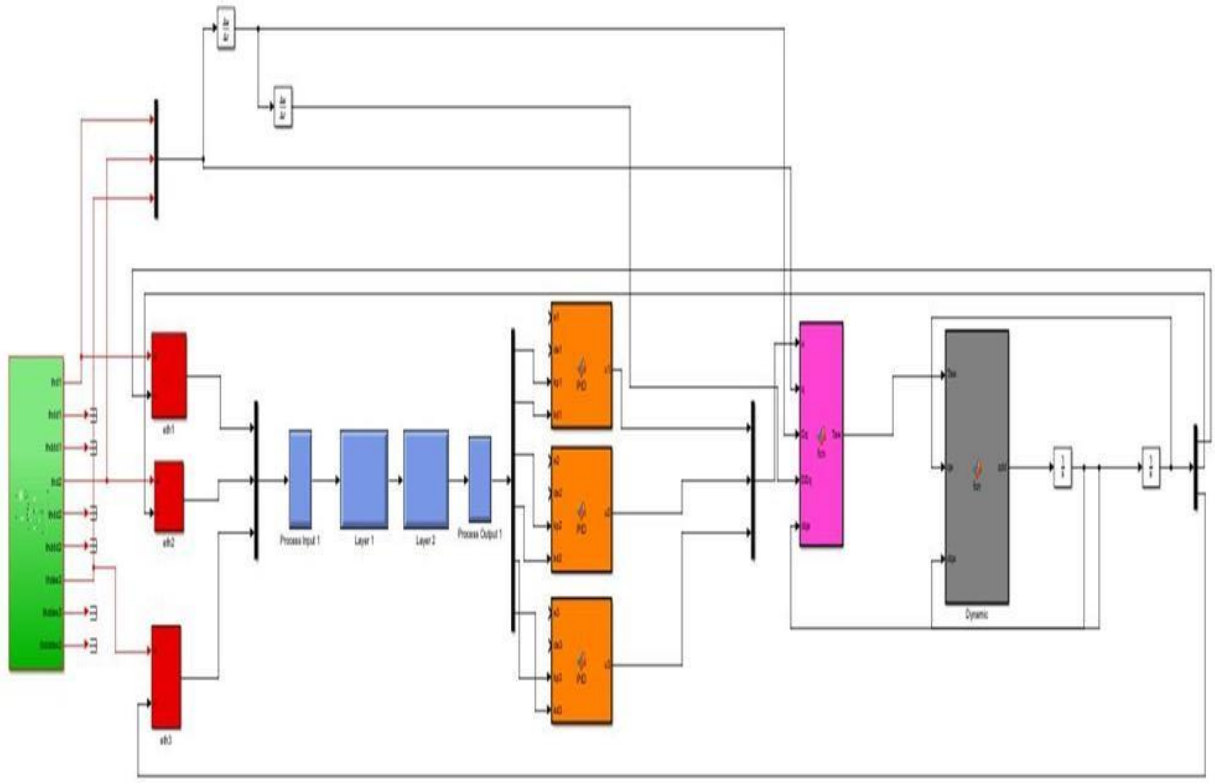

FIG. 4. DIAGRAM OF THE MATLAB/SIMULINK OF CTC-NN-GWO GOVERNING TECHNIQUE.

III. RESULR AND DISSCASSION

To establish the dynamic conduct of the resulting extracted model having (2) linkages and (3) active actuators, a shift from the home configuration to the second configuration was performed in Simulink with zero friction and zero external forces. To show the effectiveness and performance of the novel hybrid controller design for the 3-DOF MR, MATLAB programming was used to model the equations and review the results. A comparison study was conducted in this work between the results acquired from the novel hybrid controller CTC-PSO and the findings obtained from CTC-NN-GWO. The 3-DOF MR's parametric values are shown in Table II. Where m1 represents the mass of the base with the mass of three stepper motors, while m3 and m3 are the mass of two links, and M is the target mass.

TABLE II. MASS PROPERTIES OF 3-DOF MR

	mi (Kg)	***rci (mm)***	***Mass moment of inertia*** **i**		
			Ixxi (Kg.mm²)	***Iyyi***	***Izzi***
m1	3.46	[86.39;-4.09; 3.34]^T	930	378.2	43641
m2	0.25	[79.45; 0.18; -2.16]^T	170.3	892.5	862.2
m3	0.34	[132.35;-0.30; 49.90]^T	203.6	142.8	1336.3
M	0.16	[35;25;25]^T	65.6	971.1	97.13

Also, the link lengths are d_1 (110 mm), a_2 (135 mm), and a_3 (160 mm). A test was conducted for the movement of the arm for the proposed control methods. The angular displacement values were

Received 14/September/2023; Accepted 23/January/2024
 ISSN (Print) 1811-9212 *ISSN (Online) 2617-3352*

DOI: https://doi.org/10.33103/uot.ijccce.24.2.1

imposed for each joint. The base of the 3-DOF MR rotates with an angular displacement range of [0° 180°], while in the second and third arms, each joint rotates with an angle displacement of 60°.

The path planning includes rotating the second and third links at an angle of 60° and upon reaching the horizontal level. The base of the manipulator begins to rotate from 0°-180° and then stops for a specified period of time, after that, the reverse movement of the manipulator arm is repeated.

In this situation, only the CTC-PSO findings were considered, and they are expressed as follows:

The previously mentioned equation (24) is programmed and simulated in MATLAB/Simulink. The values of the gains, i.e. (K_p and K_d), are determined by trial and error, and the parameters with range [0-25] are set to:

The factors of CTC-PSO are (K_{p1} = 14.87, K_{d1} = 9.802, K_{p2} = 18.5, K_{d2} = 12.205, K_{p3}= 9.90, and K_{d3} = 6.433), whereas the factors of CTC-NN-GWO are (K_{p1} = 8.66, K_{d1} = 4.658, K_{p2} = 12.685, K_{d2} = 3.417, K_{p3} = 7.114, and K_{d3} = 8.115). Also, the PSO parameters are listed in Table III.

TABLE III. PSO PARAMETERS

Parameters	Value
Particles No.	6
Iterations Max. No	5
$c_1 = c_2$	2
Objective Function	$\frac{1}{N}\sum_{i=1}^{N}(e_x^2 + e_y^2 + e_z^2)$
W	1

The position behavior of each joint in the 3-DOF MR arm is depicted in *Fig. 5* and *6*. The first and second links begin to descend. It reaches a value of 60 degrees in roughly 4 seconds until the camera reaches the horizontal level, at which point the base of the manipulator arm is fixed. Following that, the manipulator's base moves clockwise from (0 -180) degrees. When it is reached, the method that descends the 2nd and 3rd links grabs the target (object), raises it, and returns to the starting point is repeated.

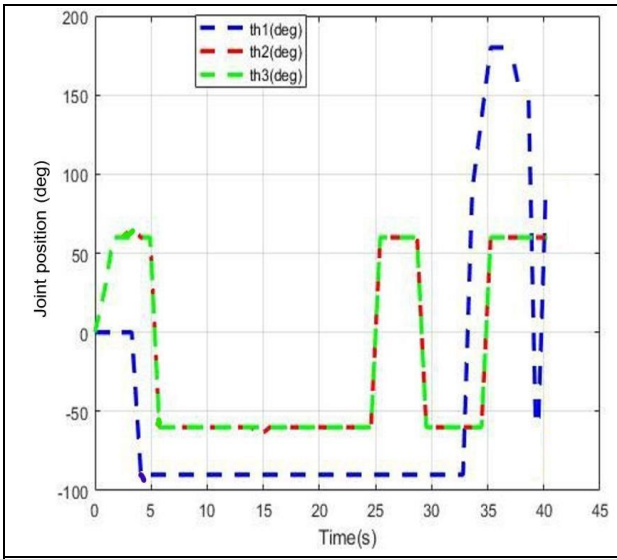

FIG. 5. THE CTC-PSO METHODOLOGY ANGULAR POSITION.

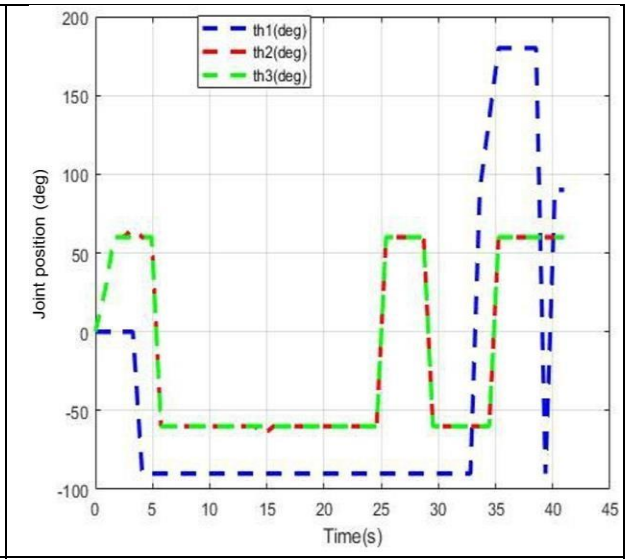

FIG. 6. THE CTC-NN-GWO METHODOLOGY ANGULAR POSITION.

Received 14/September/2023; Accepted 23/January/2024
 ISSN (Print) 1811-9212 ISSN (Online) 2617-3352

DOI: https://doi.org/10.33103/uot.ijccce.24.2.1

Fig. 7 depicts the orientation error response for 3-DOF MRs, exhibiting a virtuous response from the controller technology of CTC-PSO. And, the $e_\theta 1$ determined value at the simulation start is (- 0.29 rad), whereas $e_\theta 2$ and $e_\theta 3$ are around (1 rad). Also, the values of error steadied at roughly (∓ 0.005 rad) after (4 sec), and the values stayed virtually constant until the simulation ended. While for the second control methodology CTC-NN-GWO orientation error response for 3-DOF MR, appeared in *Fig. 8*. At the experiment starting, the maximal value of $e_\theta 1$ is (-0.29 rad), whereas $e_\theta 2$ and $e_\theta 3$ are approximately (0.15 rad) and (-0.07 rad), respectively. After about (4 sec), the error levels normalized and remained nearly constant.

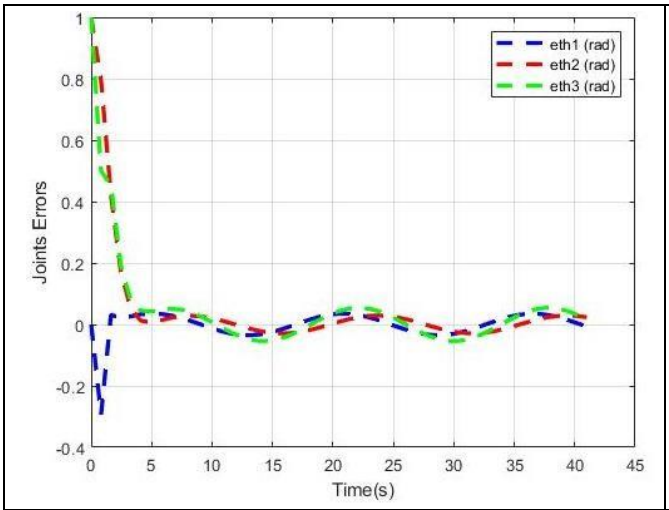

FIG. 7. ERROR OF ANGULAR POSITION FOR CTC-PSO METHODOLOGY.

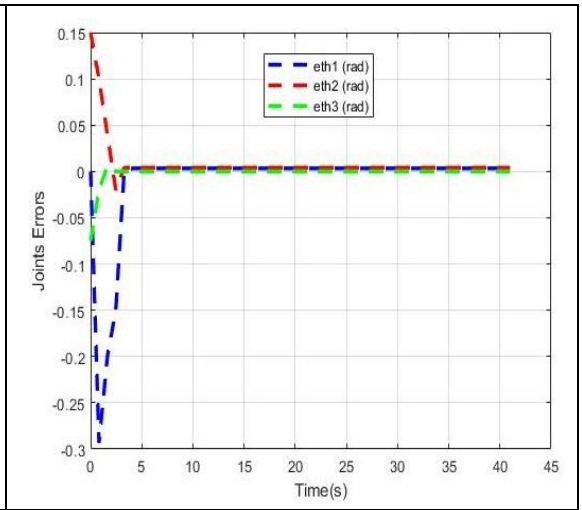

FIG. 8. ERROR OF ANGULAR POSITION FOR CTC-NN-GWO METHODOLOGY.

Fig. 9 elucidates the three-degree of freedom (3-DOF) MR joints actuator conduct. Using the CTCPSO control methodology, the torque in every joint investigating the select path planning to reach the target that ranges between (0.349 N.m) and (1.2 N.m). *Fig. 10* also displays the torque characteristic of the CTC-NN-GWO. And, the limit of torque in this situation is (0.09-0.25 N.m) and - (0.32-0.04 N.m).

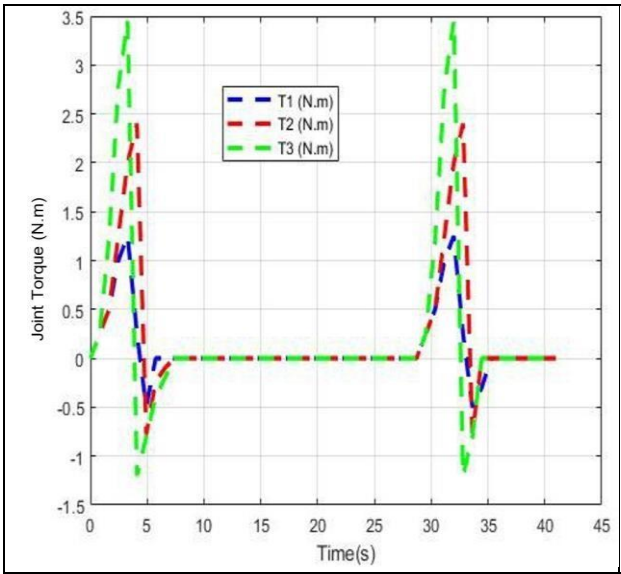

FIG. 9. THE CTC-PSO METHODOLOGY TORQUE BEHAVIOR.

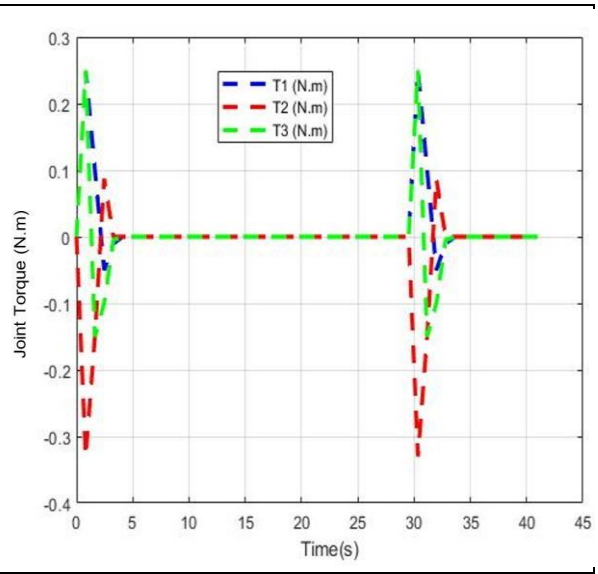

FIG. 10. THE CTC-NN.GWO METHODOLOGY TORQUE BEHAVIOR.

Received 14/September/2023; Accepted 23/January/2024
 ISSN (Print) 1811-9212 *ISSN (Online) 2617-3352*

DOI: https://doi.org/10.33103/uot.ijccce.24.2.1

IV. CONCLUSIONS

The study of path planning of 3-DOF MR is considered an important and interesting topic. In this work, a hybrid controller consisting of Computed Torque Control-Neural Network-Grey Wolf Optmasition (CTC-NN-GWO) is proposed for the path planning of 3-DOF MR. first, both kinematics and dynamic models have been derived. MATLAB programming has been used to simulate the equations and to obtain the theoretical results. A computed torque controller has been applied for compute the magnitudes of the torque that are generated from each stepper motor of the 3DOF MR. CTC has been used to compute the magnitudes of the parameters of gain (K_p) but the output from NN so that, GWO has been used to de-normalizing the output values from NN as well as to compute the optimum values of another gain parameter which is (K_d). A comparison study between the hybrid controller CTC-NN-GWO and CTC-PSO has been adopted and the results show that this hybrid controller i.e., (CTC-NN-GWO) gives results better than the results obtained from CTC-PSO because this hybrid controller minimized the path planning errors of the 3-DOF MR which are about

(1) rad in CTC-PSO for two linkes joint ,and $e_\theta 2$ and $e_\theta 3$ are approximately (0.15 rad) and (-0.07 rad), respectively in CTC-NN-GWO as well as reducing the magnitudes of the torques that generated from each motor which are between (-1.2-3.5) N.m in CTC-PSO to (-0.31-2.5) N.m in CTC-NNGWO, this improves the performance of the 3-DOF MR.

REFERENCES

[1] H. Mehdi and O. Boubaker, "Impedance Controller Tuned by Particle Swarm Optimization for Robotic Arms," Int. J. of Adv. Robot. System, Vol. 8, No. 5, pp.93 -103,2011.

[2] A. Jalali, F. Piltan, et al, "Model-Free Adaptive Fuzzy Sliding Mode Controller Optimized by Particle Swarm for Robot Manipulator," Int. J. Inf. Eng. Electron. Bus., Vol. 5, No. 1, pp. 68–78,2013.

[3] A. E. Serbencu, et al, "Particle Swarm Optimization for the Sliding Mode Controller Parameters," Proc. 29th Chinese Control Conf. CCCIEEE, pp. 1859–1864,2010.

[4] H. Mohammad Alwan and Zaid Hikmat Rashid" Kinematic Analysis and Simulation of Three Link (Open Chain) Robot Manipulator with Six DOF" Journal of Engineering and Applied Sciences, Vol.13, 1829-1834,2018.

[5] S. Manjeet, & Sathans,"Fuzzy Based Control of Two Link Robotic Manipulator and Comparative Analysis" International Conference on Communication Systems and Network Technologies 2013, doi:10.1109/csnt.2013.

[6] A. Mehiri, & R. Fareh,"Comparison study on advanced control of two 2DOF manipulator robots," International Conference on Electrical and Computing Technologies and Applications (ICECTA) IEEE,pp.1-5,2017.

[7] Song, Z., Yi, J., Zhao, D., & Li, X. "A computed torque controller for uncertain robotic manipulator systems" Fuzzy approach. Fuzzy Sets and Systems154(2), 208–226,2005.

[8] A.Sharkawy, Panagiotis Koustoumpardis" Dynamics and Computed-Torque Control of a 2-DOF manipulator Mathematical Analysis" International Journal of Advanced Science and Technology, 28 ,12, pp.201212,2019.

[9] O. O. Obadina, M. Thaha, K. Althoefer, and M. H. Shaheed, "A Modified Computed Torque Control Approach for a Master-Slave Robot Manipulator System," in Towards Autonomous Robotic Systems. TAROS, Lecture Notes in Computer Science, vol. 10965, Springer, Cham, pp. 28–39,2018.

[10] Z. Song, Jianqiang Yi, Dongbin Zhao, Xinchun Li" A computed torque controller for uncertain robotic manipulator systems: Fuzzy approach" Fuzzy Sets and Systems 154 , 208–226,2005.

[11] D. Receanu, "Modeling and Simulation of the Nonlinear Computed Torque Control in Simulink / MATLAB for an Industrial Robot," SL, vol. 10, no. 2, pp. 95–106,2013.

[12] M. W. Spong, S. Hutchinson, and M. Vidyasagar "Robot modeling and control"vol. Wiley New York, 2006.

[13] H. Mohammed. Alwan and Zaid Hikmat Rashid" Kinematic Analysis and Simulation of Three Link (Open Chain) Robot Manipulator with Six DOF" Journal of Engineering and Applied Sciences,13: 1829-1834,2018.

[14] S. L., Hassan Z. "Modeling, Simulation and Position Control of 3DOF Articulated Manipulator" IJEEI.Vol. 2, No. 3, pp. 132~140,2014.

[15] F. S. Hameed and Hassan M. Alwan "Theoretical and Experimental Study of a Multiple Degree-of-Freedom OpenChain Robotic Manipulator with Image Processing Control"phd thesis, University of Technology.Mechanical Engineering Department,pp 37-40, 2020.

Received 14/September/2023; Accepted 23/January/2024
 ISSN (Print) 1811-9212 *ISSN (Online) 2617-3352*

DOI: https://doi.org/10.33103/uot.ijccce.24.2.1

[16] M. Boukattaya, Neila Mezghani and Tarak Damak" Computed-Torque Control of a Wheeled Mobile Manipulator" Int J Robot Eng, 3:005,2018.

[17] M.A. El-Shorbagy and Aboul Ella Hassanien, "Particle Swarm Optimization from Theory to Applications", Vol.5, Issue.2,pp. 1-14,2018.

[18] S. F. Hasan, Hassan M. Alwan" Design of Hybrid Controller for the Trajectory Tracking of Wheeled Mobile Robot with Mecanum Wheels" Journal of Mechanical Engineering Research and Developments.Vol. 43, No.5, pp.400414,2021.

[19] F.L. LEWIS, S. JAGANNATHAN and A. YES¸ILDIREK "Neural Network Control of Robot Manipulators and Nonlinear Systems "Taylor &France, Book.pp175-185,1999.

[20] C Muro R Escobedo, L Spector, R. Coppinger "Wolf-pack (Canis lupus) hunting strategies emerge from simple rules in computational simulations" Behav Process;88:192–7,2011.

[21] S. Mirjalili , S Mohammad Mirjalili , A Lewis "Grey Wolf Optimizer" Advances in Engineering Software 69, 46–61,2014.

Received 14/September/2023; Accepted 23/January/2024

 ISSN (Print) 1811-9212 *ISSN (Online) 2617-3352*